



# Significantly Enhanced Dielectric Behavior of Polyvinylidene Fluoride-Barium Strontium Titanate Flexible Nanocomposite Thick Films: Role of Electric Field-Induced Effects

Sachin Jaidka<sup>1</sup> · Arun Aggarwal<sup>2</sup> · Sandeep Chopra<sup>2</sup> · Dwijendra P. Singh<sup>1</sup>

Received: 2 March 2022 / Accepted: 17 June 2022 / Published online: 9 July 2022  
© The Minerals, Metals & Materials Society 2022

## Abstract

The polyvinylidene fluoride (PVDF)-0.05Ba<sub>0.8</sub>Sr<sub>0.2</sub>TiO<sub>3</sub> (BST) nanocomposite (0.05 is the fractional weight of BST) facile thick films of thickness ~100 μm have been synthesized by tape-casting. The synthesized films are exposed to an electric field of 22 kV/mm (for different time durations, 0 min, 40 min, 50 min, and 60 min) to investigate the electric field-induced effects on dielectric and structural properties of nanocomposite thick films. Structural studies have shown that the electric field increases the β phase of PVDF in PVDF-BST nanocomposites. The most prominent effect of the applied electric field is observed in the dielectric behavior of the nanocomposite thick films. The film exposed to the electric field for 60 min has the highest dielectric constant (~25) and very low tangent loss (~0.02) at 1 kHz, whereas the unexposed film of nanocomposite has a dielectric constant of ~15 and tangent loss (~0.03). The approximated Debye relaxation theory has been used to understand the correlation between dielectric and structural observations. Analysis confirms the duration of exposure to the electric field enhances the β-phase, which causes the increase in the density of dipoles. The enhanced dielectric performance is attributed to the increased dipolar density due to modification in the structural and interfacial behavior as well as molecular motion of the dipoles in the polymeric chain.

**Keywords** BST · PVDF · polymer-ceramic nanocomposites · dielectric constant · impedance analysis

## Introduction

Polymer-based ceramic nanocomposites and their dielectric behavior have been the focus of research for the last decade due to their prospect of application in high-energy storage capacitors, embedded electronics, pulse power generation, etc.<sup>1–3</sup> There are a large number of polymers that are utilized as a matrix for this purpose, e.g. biaxially oriented polypropylene,<sup>4</sup> polyamide,<sup>5</sup> polyvinylidene fluoride (PVDF),<sup>6,7</sup> polyvinylidene fluoride-trifluoroethylene (PVDF-TrFE),<sup>8</sup> polydimethylsiloxane (PDMS)<sup>9</sup>, etc. All these polymers have a very low dielectric constant

(< 12).<sup>10,11</sup> Ceramic particles with a high dielectric constant are incorporated into the matrix of polymers in order to make polymer-based nanocomposites that consist of lead zirconate titanate (PZT) ( $\epsilon'$  ~600),<sup>12</sup> barium titanate (BaTiO<sub>3</sub>) ( $\epsilon'$  ~1700),<sup>13</sup> strontium titanate (SrTiO<sub>3</sub>) ( $\epsilon'$  ~1000),<sup>14</sup> calcium copper titanate (CCTO) ( $\epsilon'$  ~60000),<sup>13</sup> titanium oxide (TiO<sub>2</sub>) ( $\epsilon'$  ~200),<sup>15</sup> etc. The composites based on high dielectric constant ceramic materials and low dielectric constant flexible polymers have a moderate dielectric constant and low tangent loss. PVDF shows unique behavior among all dielectric polymers with its dielectric constant ~10, tangent loss ~0.05, and breakdown field ~500 MV/m.<sup>16</sup> Apart from this, its ease of processing, the existence of various crystalline phases (such as  $\alpha$ ,  $\beta$ , and  $\gamma$  crystalline phases), and associated electrical properties such as ferroelectric, piezoelectric, and pyroelectric<sup>17</sup> make it most suitable for making polymer-based ceramic nanocomposites. On the other hand, lead-free barium strontium titanate (BaSrTiO<sub>3</sub>, BST) possesses very good dielectric behavior with a large dielectric constant over a wide temperature (–173°C to 120°C) and

✉ Dwijendra P. Singh  
dpsingh@thapar.edu

<sup>1</sup> Energy Materials Lab, School of Physics and Materials Science, Thapar Institute of Engineering and Technology, Patiala, Punjab, India

<sup>2</sup> Terminal Ballistics Research Laboratory (TBRL), DRDO, Chandigarh, India

frequency (100 Hz to 1 MHz).<sup>18,19</sup> Therefore, the dielectric, structural, and energy storage behavior of PVDF-BST nanocomposites has been widely investigated.<sup>7,20,21</sup> These days, polymer-ceramic nanocomposites with a low volume/weight percentage of ceramic loading, higher dielectric constant, and low loss are required.<sup>22</sup> Several methods have been adopted to achieve high dielectric constant and low loss polymer-ceramic nanocomposites, such as a change in shape, size, and functionalization of the incorporated filler, stretching, and poling the nanocomposites, etc.<sup>20,23–25</sup> Dopamine-modified  $\text{Ba}_{0.6}\text{Sr}_{0.4}\text{TiO}_3$  (BST) nanofiber/PVDF nanocomposites are found to have much improved dielectric and energy storage behavior,<sup>18</sup> which is attributed to surface modification by dopamine and large aspect ratio of BST nanofibers. The use of a polyvinylpyrrolidone (PVP) linker layer as an adhesive in multilayered  $\text{BaTiO}_3$  nanofiber/PVDF nanocomposites is found to improve the dielectric behavior and energy storage properties,<sup>26</sup> which is caused by homogeneous surfaces due to the presence of the multilayer PVDF. The high discharge energy density in PVDF-based nanocomposites loaded with fine  $\text{Ba}_{0.6}\text{Sr}_{0.4}\text{TiO}_3$  nanofibers along with a high dielectric constant ( $\sim 22$ ) has been achieved,<sup>27</sup> which is assigned to the regulation of diameter of 1-D nanofiber and improvement of interfaces between ceramic filler and PVDF matrix. Dielectric constant and breakdown field are very important parameters for the material to be used for high-voltage capacitor applications. The higher volume/weight percentage loading of the ceramic particles in the polymer-based composites leads to a high dielectric constant, but the breakdown field decreases. Dielectric properties of polymer-based nanocomposites are improved by different methods of processing,<sup>28,29</sup> interfacial modification,<sup>18,27</sup> etc. The high value of the dielectric constant is usually obtained for higher loading of ceramic nanoparticles as well as poling at a very high voltage for a longer duration.<sup>23,30–32</sup> The processing techniques adopted for synthesizing nanocomposite thick films include tape casting, solution casting, and spin casting.<sup>28,33–35</sup> The tape-casting method produces large-area nanocomposite thick films of uniform thickness and ensures homogeneous dispersion of ceramic nanoparticles. The application of electric field is capable of rotating a randomly aligned dipole in the direction of the electric field,<sup>36</sup> which may change the crystalline phases of PVDF in PVDF- $\text{Ba}_{0.8}\text{Sr}_{0.2}\text{TiO}_3$  nanocomposite thick films. Therefore, the motivation of the present work is based on the fact that the exposure of PVDF- $\text{Ba}_{0.8}\text{Sr}_{0.2}\text{TiO}_3$  nanocomposite thick films to an electric field effects the structural and dielectric properties at very small fractional loading of  $\text{Ba}_{0.8}\text{Sr}_{0.2}\text{TiO}_3$  nanoparticles in the PVDF matrix.

The present paper reports the electric field-induced effect on the dielectric and structural behavior of tape-cast PVDF- $\text{Ba}_{0.8}\text{Sr}_{0.2}\text{TiO}_3$  nanocomposite thick films at very small loading of  $\text{Ba}_{0.8}\text{Sr}_{0.2}\text{TiO}_3$  nanoparticles in the PVDF matrix, which could be adopted as an efficient way to modify and tune the dielectric behavior of nanocomposites.

## Material and Measurements

$\text{Ba}_{0.8}\text{Sr}_{0.2}\text{TiO}_3$  (BST) nanopowder was prepared by a hydrothermal method.<sup>37</sup> A detailed flowchart for the synthesis of BST nanopowder is shown in Fig. 1. Polyvinylidene fluoride (PVDF)-BST nanocomposite film with 5 wt% loading of BST was prepared by tape casting using a TMAX tape-casting unit. Initially, PVDF (procured from Alfa Aesar) was dissolved in *N,N*-dimethylformamide (DMF). The solution mixture of PVDF and DMF was stirred for 1.5 h at room temperature via mechanical stirring. Then 5 wt% of BST powder was added to this PVDF-DMF solution. To get the proper dispersion of BST nanoparticles in the PVDF polymer matrix, the solution containing BST nanopowder and PVDF in DMF was subjected to sonication. The sonicated solution was stirred for 5–6 h at 60°C, making the solution viscous. The viscous solution was poured on the tape-casting bed (pre-set at a temperature of 60°C), and a thick film (thickness  $\sim 100$   $\mu\text{m}$ ) was made using a doctor blade. After 1 h, the film was peeled off and put in a vacuum oven at 150°C to evaporate the excess DMF. The dried nanocomposite film was then cut into small pieces, which were subjected to an electric field of 22 kV/mm for 40 min, 50 min, and 60 min, respectively. The electric field was applied using a Danbridge 30 kV Non-Destructive Insulation Tester (Denmark). A schematic diagram showing the electric field measurements is shown in Fig. 2.

The x-ray diffraction (XRD) patterns of the PVDF-BST nanocomposite films were recorded by a PANalytical X'Pert Pro MPD diffractometer with  $\text{Cu-K}\alpha$  radiation ( $\lambda = 1.54$  Å). A scanning electron microscope (JEOL JSM-6510LV) was used for detecting the surface morphology of PVDF-BST nanocomposite samples, and a transmission electron microscope (TEM) (JEOL 2100 F) operating at 200 kV was used to observe the microstructural and morphological features of BST powder. An Agilent Resolution Pro Cary 660 spectrometer recorded Fourier transform infrared (FTIR) spectra of the PVDF-BST nanocomposite films. A silver contact of 5-mm diameter was deposited on both sides of the films for measuring the dielectric behavior. The dielectric properties were measured using a Wayne Kerr 6500B precision impedance analyzer in the frequency range of 100 Hz to 10 MHz at room temperature.

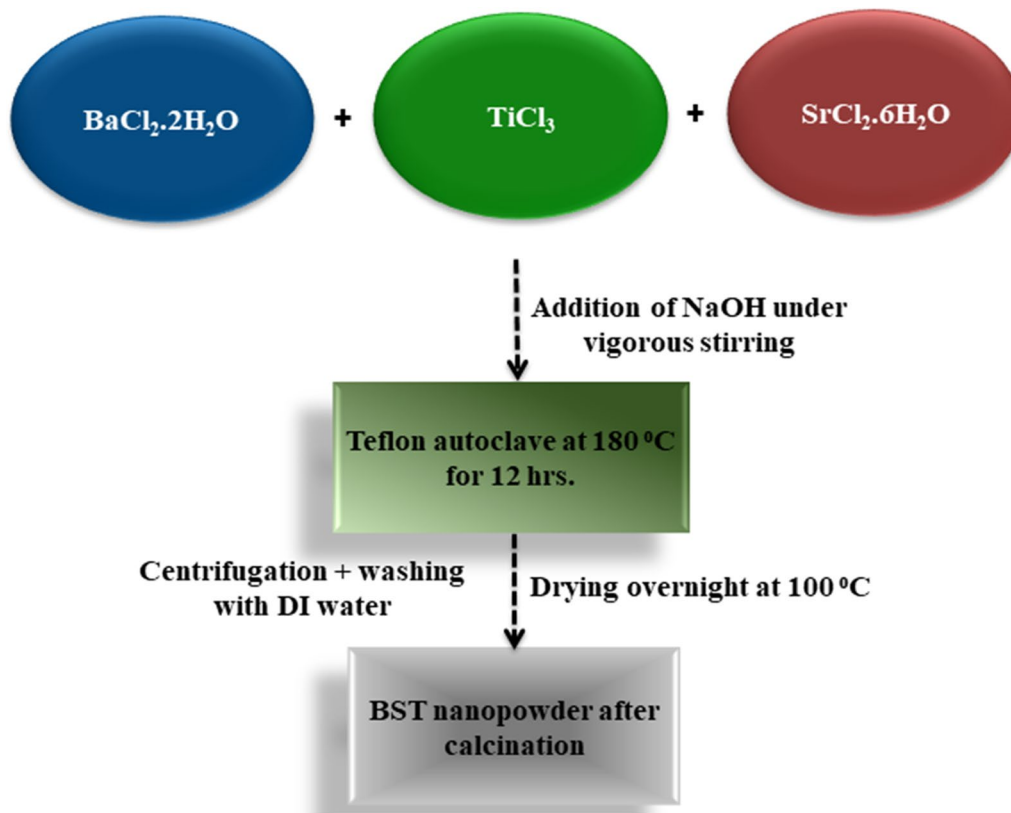


Fig. 1 Detailed flowchart for the synthesis of BST nanopowder.

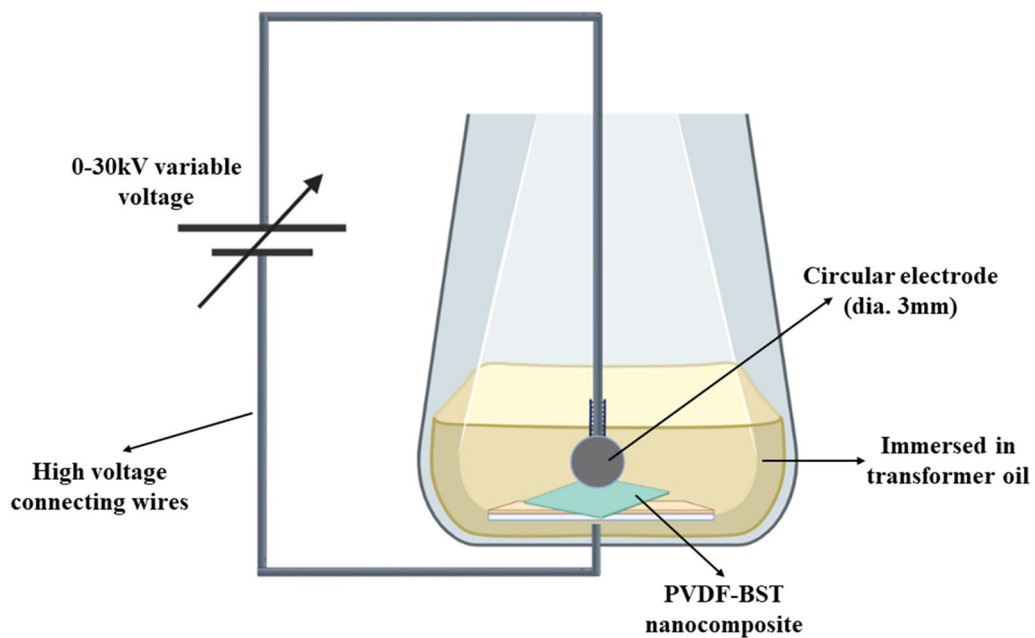
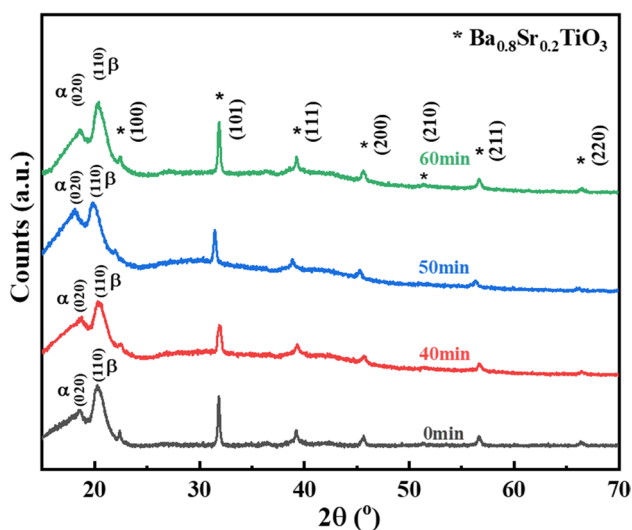


Fig. 2 Schematic diagram showing the electric field measurement setup.

## Results and Discussion

### X-ray Diffraction (XRD)

Figure 3 shows the XRD patterns of PVDF-BST nanocomposite films subjected to an external electric field of 22 kV/mm for different time durations. The  $\alpha$  and  $\beta$  crystalline phases for all films has been observed. The  $\beta$  phase with (110) plane at  $20.4^\circ$  and  $\alpha$  phase with (020) plane of PVDF at  $18.5^\circ$  (JCPDS card no. 38-1638) were observed. The diffraction peaks at  $22.5^\circ$ ,  $31.8^\circ$ ,  $39.3^\circ$ ,  $45.6^\circ$ ,  $51.3^\circ$ ,  $56.8^\circ$ , and  $66.4^\circ$  correspond to (100), (101), (111), (200), (210), (211), and (220) planes of BST with a tetragonal crystal structure (JCPDS card no. 44-0093), lattice parameters  $a = b = 0.3977$  nm,  $c = 0.3988$  nm and average crystallite size of  $\sim 19$  nm (as discussed in Table I), which are observed for all the PVDF-BST nanocomposite films.<sup>20,38</sup> The peak position, crystallite size, FWHM, and d-spacing of BST nanoparticles calculated from the XRD pattern using an X'Pert HighScore Plus are shown in Table I. The average crystallite size is  $\sim 19$  nm, agreeing with the FESEM and TEM studies (discussed later in the text). So the peaks of  $\text{Ba}_{0.8}\text{Sr}_{0.2}\text{TiO}_3$  and PVDF are observed in all the nanocomposite films, confirming the incorporation of BST nanoparticles in the PVDF polymer matrix.<sup>39,40</sup> But the duration of electric field application on PVDF-BST nanocomposite thick films affects the intensity of peaks corresponding to  $\alpha$  and  $\beta$  phases of PVDF. With the increase in the time duration of the applied electric field, the intensity of the peak corresponding to the  $\alpha$  phase at  $18.5^\circ$  decreases, whereas for the  $\beta$  phase at  $20.4^\circ$ , the intensity increases. The peak of the  $\beta$  phase for the nanocomposite films with exposure to the electric field for 50 min and 60



**Fig. 3** X-ray diffraction patterns of PVDF- $\text{Ba}_{0.8}\text{Sr}_{0.2}\text{TiO}_3$  nanocomposites exposed to the electric field for different time durations.

min is more intense than the peak for the film with a lower duration of exposure to the electric field. The XRD studies confirm that the electric field induces the enhancement of the  $\beta$  phase in PVDF-BST nanocomposite thick films. Since x-ray diffraction only shows the probable evolution of the  $\beta$  phase induced by the electric field, Fourier transform infrared spectroscopy studies will further confirm these findings.

### Fourier Transform Infrared Spectroscopy (FTIR)

Figure 4 shows the FTIR absorption spectra of PVDF-BST nanocomposite films in the range  $1500\text{--}400\text{ cm}^{-1}$ . The formation of the  $\beta$  phase of PVDF is observed at wavenumbers of  $429\text{ cm}^{-1}$ ,  $508\text{ cm}^{-1}$ ,  $835\text{ cm}^{-1}$ ,  $874\text{ cm}^{-1}$ ,  $1166\text{ cm}^{-1}$ ,  $1230\text{ cm}^{-1}$ ,  $1278\text{ cm}^{-1}$ , and  $1401\text{ cm}^{-1}$ .<sup>41</sup> The characteristic peaks of the  $\alpha$  and  $\beta$  phases of PVDF are summarized in Table II. The absorption band at  $606\text{ cm}^{-1}$  corresponding to the  $\alpha$  phase is due to the rocking vibration of  $\text{CF}_2$  group, whereas the band

**Table I** Peak position, crystallite size, d-spacing and FWHM of BST nanoparticles calculated from XRD pattern

S. No.	Peak pos. [ $^\circ 2\theta$ ]	FWHM [ $^\circ 2\theta$ ]	d-spacing [ $\text{\AA}$ ]	Crystallite size [nm]
1	22.5	0.247	3.984	$\sim 34$
2	31.8	0.370	2.811	$\sim 23$
3	39.3	0.442	2.290	$\sim 19$
4	45.6	0.542	1.987	$\sim 16$
5	56.8	0.680	1.619	$\sim 13$
6	66.4	0.827	1.406	$\sim 11$

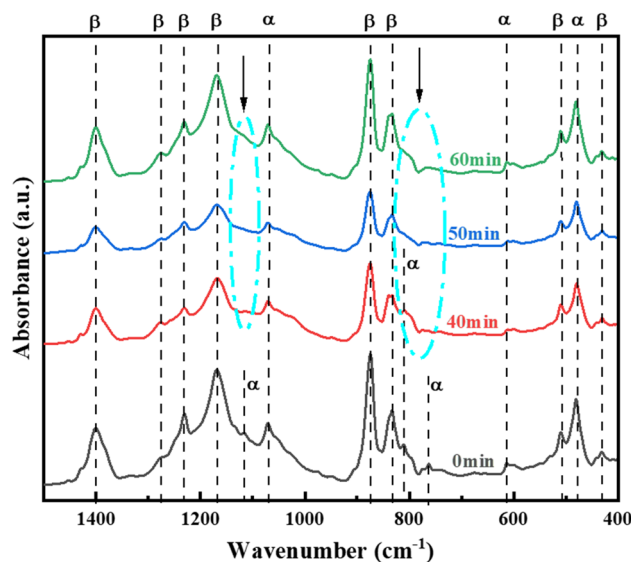


**Fig. 4** Fourier transform infrared absorption spectra of PVDF- $\text{Ba}_{0.8}\text{Sr}_{0.2}\text{TiO}_3$  nanocomposites exposed to the electric field for different time durations.

**Table II** FTIR characteristic diffraction peaks of  $\alpha$  and  $\beta$  phase of PVDF

Crystalline phases	$\alpha$	$\beta$
Wavenumber (cm <sup>-1</sup> )	478	429
	606	508
	763	835
	810	874
	1068	1166
	1112	1230
		1278
		1401

at 763 cm<sup>-1</sup> is due to a mixture of CF<sub>2</sub> bending and GGG skeletal vibrations.<sup>42</sup> The peaks of the  $\alpha$  phase corresponding to absorption bands present at 763, 810, and 1112 cm<sup>-1</sup> are absent in 50 min and 60 min samples, whereas the intensity of absorption bands corresponding to the  $\beta$  phase at 874 and 1166 cm<sup>-1</sup> increases. These studies confirm the formation of the  $\beta$  crystalline phase due to exposure to the electric field. The FTIR results were used to find the relative fraction of the  $\beta$  phase using absorption peaks of  $\alpha$  and  $\beta$  phases, which is validated using the Beer-Lambert law. Accordingly, the relative fraction of the  $\beta$  phase is given by<sup>43,44</sup>:

$$F(\beta) = \frac{X_{\beta}}{X_{\alpha} + X_{\beta}} = \frac{A_{\beta}}{(K_{\beta}/K_{\alpha})A_{\alpha} + A_{\beta}} = \frac{A_{\beta}}{1.3A_{\alpha} + A_{\beta}} \quad (1)$$

where  $X_{\alpha}$  and  $X_{\beta}$  in Eq. 1 represents the mass fraction of  $\alpha$  and  $\beta$  phases,  $A_{\alpha}$  and  $A_{\beta}$  represent the absorbance at 835 cm<sup>-1</sup> and 763 cm<sup>-1</sup>, respectively and the absorption coefficients are expressed by  $K_{\alpha}$  (6.1x10<sup>4</sup> cm<sup>2</sup> mol<sup>-1</sup>) and  $K_{\beta}$  (7.7x10<sup>4</sup> cm<sup>2</sup> mol<sup>-1</sup>) at that particular wavenumber, respectively.<sup>43</sup>

According to Eq. 1, it can be seen that the F( $\beta$ ) values of the 0 min, 40 min, 50 min, and 60 min samples are 33.32%, 47.50%, 50.19%, and 54.49%, respectively. The observed results are further corroboration of the evolution of the  $\beta$  phase in PVDF of PVDF-BST nanocomposites due to the increase of time duration of exposure to the electric field. The variation in the content of the  $\beta$  phase fraction with time duration to the electric field exposure for PVDF-BST nanocomposites is shown in Fig. 8.

### Field Emission Scanning Electron Microscopy (FESEM) and Transmission Electron Microscopy (TEM) Analysis

Figure 5a shows the FESEM of the Ba<sub>0.8</sub>Sr<sub>0.2</sub>TiO<sub>3</sub> (BST) powder, which shows the agglomerates of the nanoparticles.

The inset of Fig. 5a shows the transmission electron microscopy (TEM) image of BST, which confirms the formation of nanoparticles in the range of 15-20 nm. The particle size distribution curve is shown in Fig. 5b. Figure 5c shows the fringe pattern of BST, which confirms the formation of BST with the separation between lattice planes of 0.18 nm corresponding to the [101] plane. The selected area electron diffraction (SAED) pattern of the synthesized BST powder clearly shows [100] and [101] planes in Fig. 5d,<sup>38</sup> which matches with the XRD of BST powders. Figure 5e shows the surface scanning electron micrograph (SEM) revealing the homogeneous distribution of BST nanoparticles in the PVDF polymer matrix. This uniform distribution of ceramic particles in the polymer matrix ensures a good quality PVDF-BST nanocomposite thick film with a uniform dielectric constant.

### Dielectric Studies

The electric field-induced effect on the dielectric properties of PVDF-BST nanocomposites is very important in its application for various purposes. The BST nanoparticle will experience a much lower field as compared to the polymer PVDF by virtue of its high dielectric constant.<sup>45,46</sup> The XRD and IR studies have already confirmed the electric field-induced evolution of the  $\beta$  phase in PVDF-BST nanocomposites. The variation of dielectric constant ( $\epsilon'$ ) with frequency for the PVDF-BST nanocomposite films exposed to the electric field of 22 kV/mm for different time durations is shown in Fig. 6a. The dielectric constant is found to increase with the increase in the duration of the applied electric field. But the frequency from where the dielectric constant starts decreasing shifts towards lower values with an increase in the time duration of the applied electric field. A decrease in frequency is associated with the increase of dipolar relaxation time, which might be due to the decrease of mobility of the dipoles/charge carriers in the polymeric chain or polymeric chain as a whole. Although the value of dielectric constant for the PVDF-BST nanocomposite exposed to the electric field of 22 kV/mm for 60 min is highest, i.e., ~25 at 1 kHz, the trend of variation is found to be different.

All PVDF-BST nanocomposites show nearly constant  $\epsilon'$  in the frequency range 100 Hz-100 kHz. The high values of  $\epsilon'$  in this frequency range can be ascribed to interfacial polarization present due to the difference in dielectric constant values of the filler (i.e., BST) and the polymer matrix (i.e., PVDF).<sup>47</sup> The decrease in  $\epsilon'$  with increasing frequency (>100 kHz) is due to lag in the frequency of the applied field and the dipolar orientation in PVDF-BST nanocomposites.<sup>48</sup> The PVDF-BST nanocomposite consisting of 5% (w/w) loading of BST nanoparticles exhibits the highest dielectric constant (~25) and very low tangent



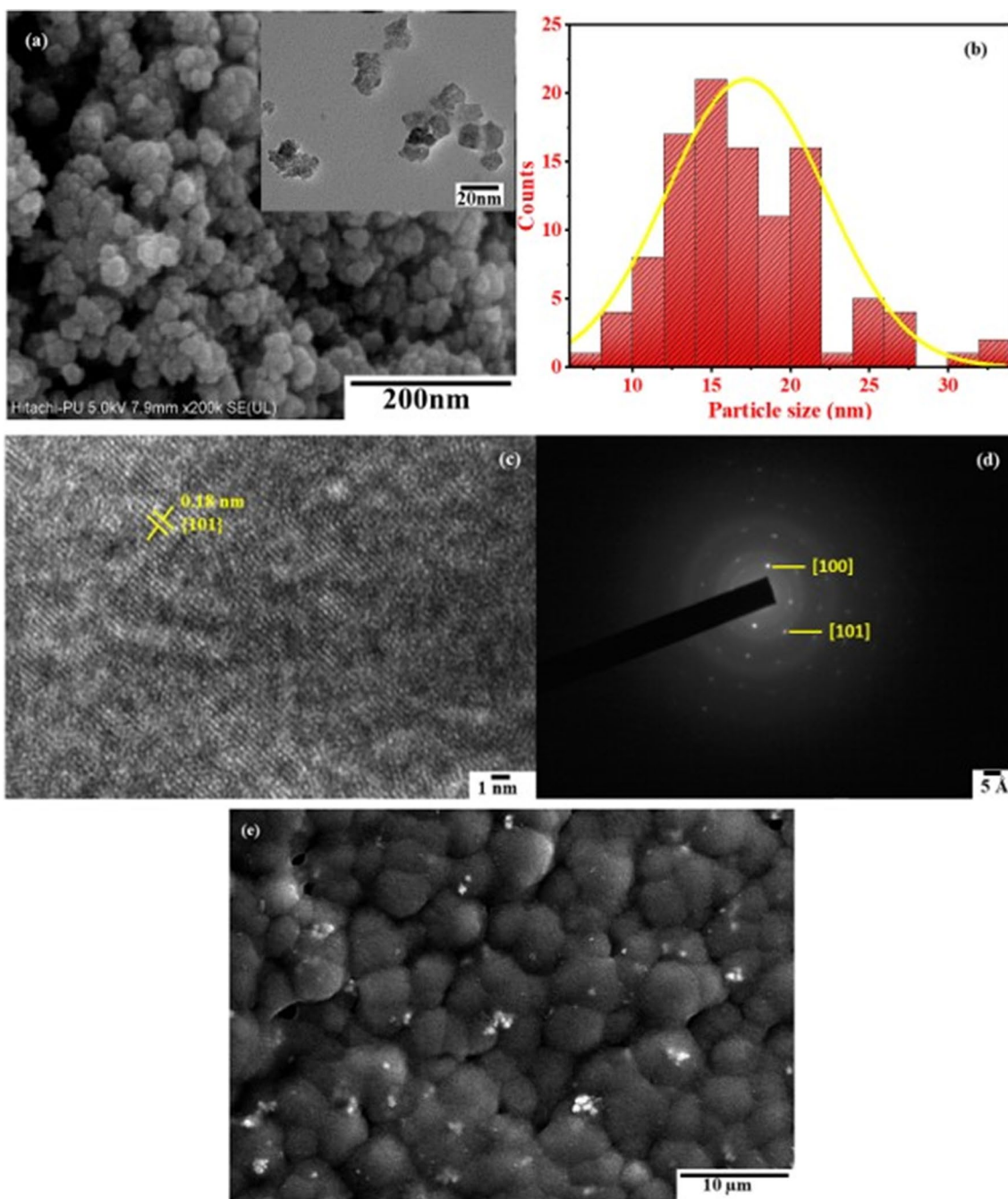


**Fig. 5** (a) Field emission scanning electron micrograph (FESEM) of  $\text{Ba}_{0.8}\text{Sr}_{0.2}\text{TiO}_3$  powder (inset: Transmission electron microscopy image confirming the particle size), (b) Particle size distribution curve for  $\text{Ba}_{0.8}\text{Sr}_{0.2}\text{TiO}_3$  particles, (c) Lattice fringe pat-

tern of  $\text{Ba}_{0.8}\text{Sr}_{0.2}\text{TiO}_3$ , (d) Selected area electron diffraction pattern of  $\text{Ba}_{0.8}\text{Sr}_{0.2}\text{TiO}_3$  powder, and (e) SEM micrograph of PVDF- $\text{Ba}_{0.8}\text{Sr}_{0.2}\text{TiO}_3$  nanocomposite.

loss (0.02). A comparative table of observed dielectric constant and tangent loss is shown in Table III. The observed high value of dielectric constant with an increase of exposure time of applied electric field is ascribed to:

- i. The evolution of the  $\beta$  phase of PVDF in PVDF-BST nanocomposites and decrease of mobility of the polymeric chain.
- ii. Enhancement of the  $\beta$  phase leads to an increase in the dipolar density.

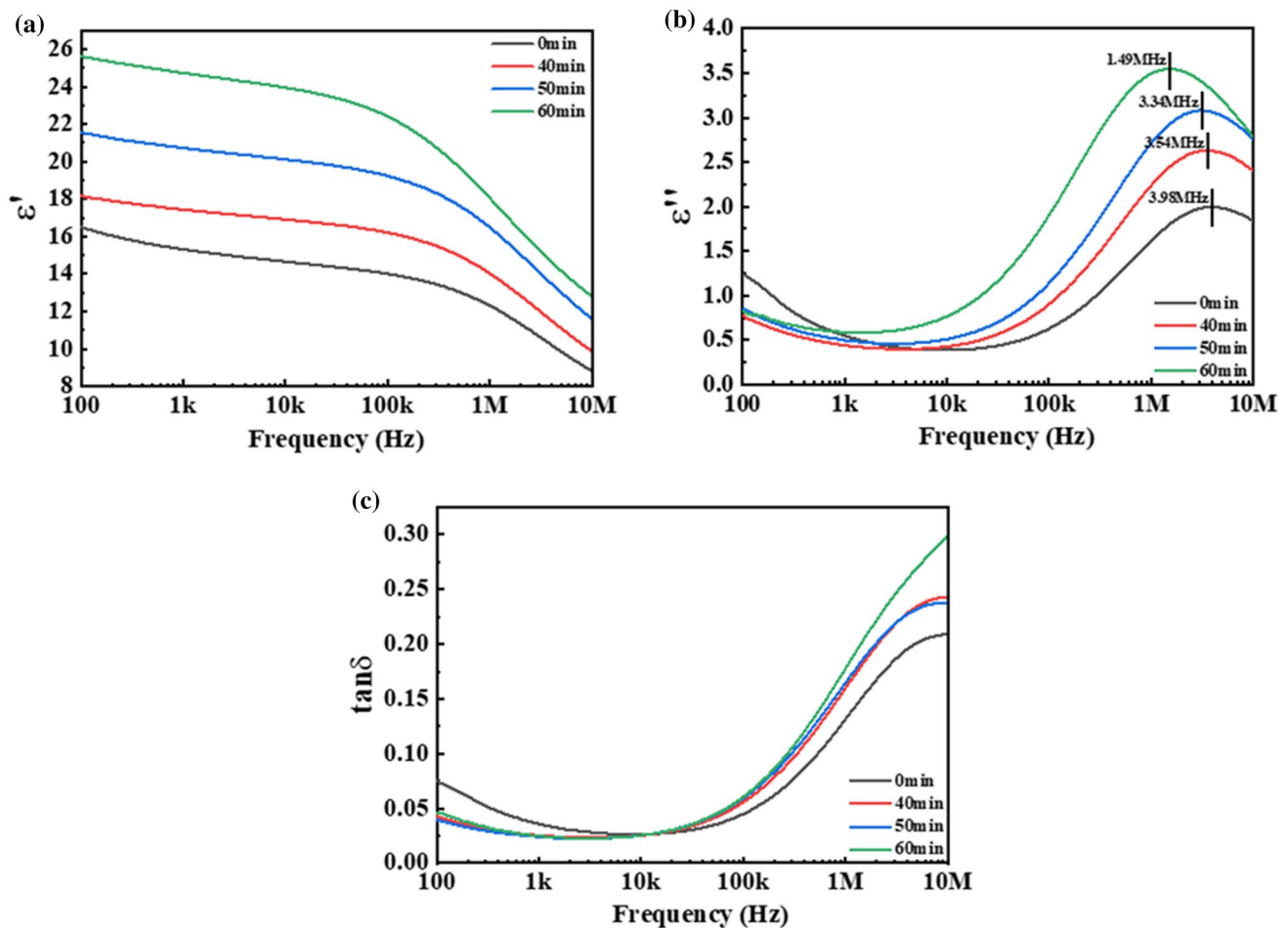


**Fig. 6** Frequency-dependent (a) real, (b) imaginary dielectric constant and (c) tangent loss for PVDF-Ba<sub>0.8</sub>Sr<sub>0.2</sub>TiO<sub>3</sub> nanocomposite films.

**Table III** Comparative data for dielectric constant and tangent loss of PVDF-BST nanocomposites

	Year	Material	Dielectric (1 kHz)	Loss (1 kHz)	References
1.	2012	PVDF-BST	~12.5 (at 4.4% loading)	~0.04	18
2.	2015	PVDF-ST	~12.5 (at 5% loading)	~0.04	53
3.	2016	PVDF-BST	~16 (at 5% loading)	~0.04	19
4.	2017	PVDF-BT	~13 (at 5% loading)	~0.05	29
5.	2018	PVDF-BST	~21 (at 5% loading)	~0.04	20
6.	2020	PVDF-BT	~13 (at 5% loading)	~0.05	54
7.	Present work	PVDF-BST	~25 (at 5% loading)	~0.02	Present work

iii. The application of the electric field promotes the accumulation of space charges in the polymer near the interface, which increases the internal field in the ceramics phase and removes the discontinuity of the electric displacement at the interface, leading to an increase in the dielectric constant.

Significant enhancement in the dielectric properties is resulting from the interfaces between the BST/PVDF and

CH<sub>2</sub>-CF<sub>2</sub> in PVDF. These interfaces might form the parallel capacitance network, which enhances the dielectric constant.<sup>49</sup> The tangent loss, imaginary component of the dielectric constant, and Cole-Cole analysis have also been carried out in order to get more insight into the physical phenomena taking place due to the application of the electric field. The tangent loss (Fig. 6c) decreases in the range of 100 Hz–10 kHz due to molecular motions in the crystalline regions of PVDF ( $\alpha$  relaxation),<sup>50</sup> whereas increased tangent loss for the frequencies greater than 100 kHz could

be caused by  $\beta$ -relaxation effects in the copolymer, which arise from the micro-Brownian motion of non-crystalline chain segments.<sup>45,46,48,51</sup> The values of dielectric constant and tangent loss at 1 kHz are summarized in Table IV.

The variation of the imaginary part of dielectric constant ( $\epsilon''$ ) with frequency is shown in Fig. 6b, indicating almost similar behavior as that of tangent loss. Initially, the decrease of  $\epsilon''$  up to a frequency of 10 kHz is observed, which is caused by molecular motion in the crystalline region of PVDF.<sup>50</sup> But for frequencies greater than 10 kHz,  $\epsilon''$  increases, and it attains a peak at different frequencies for the PVDF-BST nanocomposite films exposed to the electric field for different time durations. This peak shifts towards the lower frequency with an increase in the time duration of electric field exposure, showing a complete correlation with frequency from where dielectric constant starts decreasing. The peak in  $\epsilon''$  might be originating from

**Table IV** Dielectric constant and tangent loss at 1 kHz for PVDF-BST nanocomposites

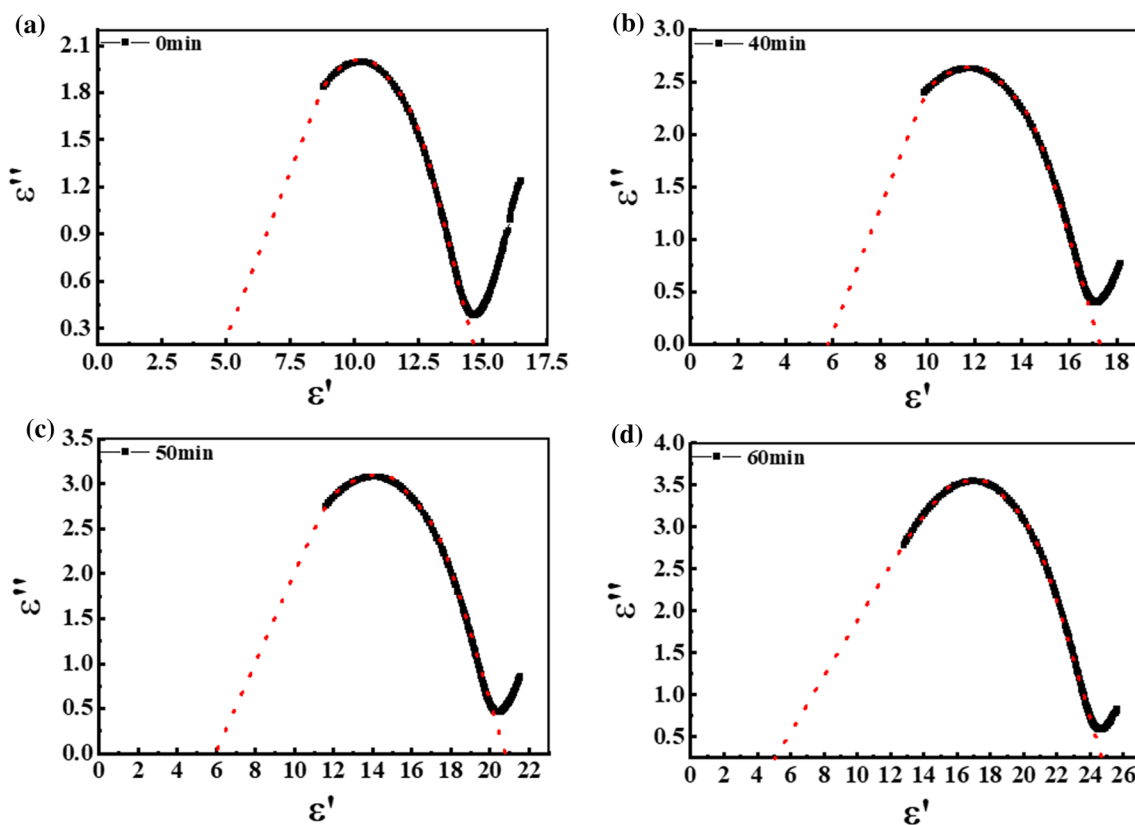
Sample	0 min	40 min	50 min	60 min
$\epsilon'$ (1 kHz)	~15	~17	~21	~25
Tan $\delta$ (1 kHz)	~0.04	~0.03	~0.02	~0.02

the micro-Brownian motion of the amorphous chain segment,<sup>47,48</sup> which controls the charge carrier transport. The relaxation of dipoles becomes slower with the increased exposure time of the applied electric field; that's why the peak at the higher frequency is shifting towards a lower frequency.

Cole-Cole analysis has been widely used for understanding dielectric relaxation by showing the plot between the real and imaginary parts of dielectric constant. According to Debye relaxation theory (Eq. 2), the real part and imaginary part of dielectric constant are related as:

$$(\epsilon' - \epsilon_\infty)^2 + (\epsilon'')^2 = (\epsilon_0 - \epsilon_\infty)^2 \quad (2)$$

where  $\epsilon_\infty$ ,  $\epsilon_0$  are dielectric constant at infinite frequency and static dielectric constant, respectively. The difference of  $\epsilon_0$  and  $\epsilon_\infty$ , i.e.,  $\Delta\epsilon$  measures the dielectric strength. Figure 7 shows the Cole-Cole plot of PVDF-BST nanocomposites exposed to the electric field for different durations. The absence of complete semicircles indicates that Debye relaxation is not exactly taking place in PVDF-BST nanocomposites. Therefore, approximated Debye relaxation is used to understand the relaxation process in PVDF-BST nanocomposites. The respective values of the central frequency of

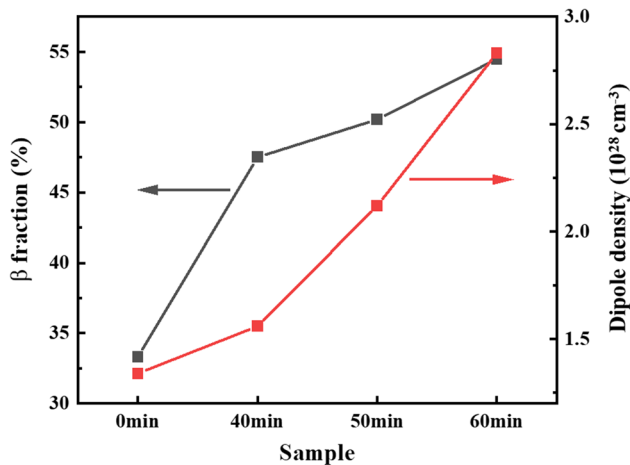


**Fig. 7** Cole-Cole plots for PVDF-  $\text{Ba}_{0.8}\text{Sr}_{0.2}\text{TiO}_3$  nanocomposites exposed to the electric field for different time durations.



**Table V** Dielectric strength,  $\beta$  fraction, the number density of dipoles, and relaxation time for PVDF-BST nanocomposites

Sample	Dielectric strength ( $\Delta\epsilon$ )	$\beta$ fraction (%)	Number density of dipoles (N, in $\text{cm}^{-3}$ )	Relaxation time ( $\tau$ , in s)
0 min	9.5	33.32	$1.34 \times 10^{28}$	$4.08 \times 10^{-8}$
40 min	11	47.5	$1.56 \times 10^{28}$	$4.54 \times 10^{-8}$
50 min	15	50.19	$2.12 \times 10^{28}$	$4.82 \times 10^{-8}$
60 min	20	54.49	$2.83 \times 10^{28}$	$1.13 \times 10^{-7}$

**Fig. 8** Variation of  $\beta$  fraction and number density of dipoles for PVDF- $\text{Ba}_{0.8}\text{Sr}_{0.2}\text{TiO}_3$  nanocomposites exposed to the electric field for different time durations.

approximated semicircles are found to be 3.9 MHz, 3.5 MHz, 3.3 MHz, and 1.4 MHz for PVDF-BST nanocomposites exposed to the electric field for 0 min, 40 min, 50 min, and 60 min, respectively. These observed values are similar to the observed peak in the variation of the imaginary part of dielectric constant (Fig. 6c). The relaxation time (i.e.,  $\tau = \frac{1}{2\pi f_{\max}}$ ) is found to increase with the increase of time duration of exposure of the electric field, which might arise due to an increase in the motion of the charge carrier at the amorphous crystalline interface of PVDF in PVDF-BST nanocomposites. The dielectric strength  $\Delta\epsilon$  ( $\epsilon_0 - \epsilon_\infty$ ) estimated from Cole-Cole plots for different time durations of the applied electric field are given in Table V. The number density of dipoles (N) contributing to the dipolar relaxation process can be estimated using the following equation:

$$\Delta\epsilon = \frac{N\mu^2 \sin^2 \frac{\alpha}{2}}{3\epsilon_0 kT} \quad (3)$$

where,  $\Delta\epsilon$ , N,  $\mu$ ,  $\alpha$ , k,  $\epsilon_0$  and T are dielectric strength, the number density of dipoles, dipole moment, the angle between dipole moments in two possible directions, Boltzmann's constant, absolute dielectric constant and the absolute temperature, respectively. Modifying this equation for PVDF-BST nanocomposites, Eq. 3 becomes:

$$\Delta\epsilon = \frac{N}{3\epsilon_0 kT} \left( \mu_1^2 \sin^2 \frac{\alpha_1}{2} + \mu_2^2 \sin^2 \frac{\alpha_2}{2} \right) \quad (4)$$

where  $\mu_1$  and  $\mu_2$  represent the dipole moment of prominent dipoles present in the ceramic and polymeric phases of PVDF-BST nanocomposites. For the polar  $-\text{CF}_2-$  groups in PVDF,  $\mu_1 = 1.66$  Debye and  $\alpha_1 = 105.3^\circ$ , while for polar tetragonal phase for BST,  $\mu_2 = 2.30$  Debye and  $\alpha_2 = 180^\circ$ .<sup>52</sup> The obtained number density of dipoles (N) for all the samples is listed in Table V. The number density of dipoles for the pristine sample was  $1.34 \times 10^{28} \text{ cm}^{-3}$ , which increased up to  $2.83 \times 10^{28} \text{ cm}^{-3}$  for the nanocomposite exposed to the electric field for 60 min. The variation of dipolar density along with  $\beta$  phase of PVDF for the PVDF-BST nanocomposites exposed to the electric field for different time duration are shown in Fig. 8. The density of dipoles in PVDF-BST nanocomposites thick films exposed to the electric field for 60 min have become more than double as compared to pristine film, which is attributed to the evolution of  $\beta$  phase of PVDF in PVDF-BST nanocomposite.

## Conclusion

The flexible polyvinylidene fluoride (PVDF)- $\text{Ba}_{0.8}\text{Sr}_{0.2}\text{TiO}_3$  (BST) nanocomposite thick films of thickness  $\sim 100 \mu\text{m}$  have been synthesized by tape casting. A detailed study of the electric field-induced effect on dielectric and structural properties of PVDF-BST nanocomposite thick films has been carried out. The XRD and IR studies reveal the evolution of the  $\beta$  phase of PVDF for the PVDF-BST nanocomposites. The dielectric constant at 1 kHz for the films exposed to the electric field for 60 min is increased up to  $\sim 25$  as compared to  $\sim 15$  for unexposed films, whereas the tangent loss does not exhibit significant change. The significant enhancement in the dielectric constant is attributed to the evolution of the  $\beta$  phase in PVDF and enhancement in dipolar density due to modification in the structural and interfacial behavior as well as molecular motion of the dipoles in the polymeric chain. Electric field-induced modification of dielectric properties (i.e. high dielectric constant and low tangent loss) could be adopted as an effective strategy for the development of flexible nanocomposite

films with very low loading of ceramic filler for different electronic applications.

**Acknowledgments** The authors are thankful to the Terminal Ballistic Research Laboratory (TBRL), DRDO, for providing financial assistance (TBRL/CARS/79/2017). The authors are also grateful to Dr. Amit L. Sharma, Scientist, CSIO-CSIR, Chandigarh, for XRD and IR measurements.

**Author contributions** **SJ:** Methodology, Validation, Formal analysis, Investigation, Writing (original draft). **AA:** Resources, Formal analysis **SC:** Resources, Formal analysis. **D.S.:** Conceptualization, Validation, Formal analysis, Writing (review and editing), Supervision.

**Data availability** The data sets generated during and/or analyzed during the current study are available from the corresponding author on reasonable request.

**conflict of interest** The authors declare that they have no conflict of interest.

## References

- H. Hu, F. Zhang, S. Luo, W. Chang, J. Yue, and C.-H. Wang, Recent Advances in Rational Design of Polymer Nanocomposite Dielectrics for Energy Storage. *Nano Energy* 74, 104844 (2020).
- V. Jella, S. Ippili, J.H. Eom, S.V.N. Pammi, and J.S. Jung, A Comprehensive Review of Flexible Piezoelectric Generators Based on Organic-Inorganic Metal Halide Perovskites. *Nano Energy* 57, 74 (2019).
- M. Safaei, H.A. Sodano, and S.R. Anton, A Review of Energy Harvesting Using Piezoelectric Materials: State-of-the-Art a Decade Later (2008–2018). *Smart Mater. Struct.* 28, 113001 (2019).
- M.-S. Zheng, Y.-T. Zheng, J.-W. Zha, Y. Yang, P. Han, Y.-Q. Wen, and Z.-M. Dang, Improved Dielectric, Tensile and Energy Storage Properties of Surface Rubberized BaTiO<sub>3</sub>/Polypropylene Nanocomposites. *Nano Energy* 48, 144 (2018).
- I. Hammami, H. Hammami, J. Soulestin, M. Arous, and A. Kallel, Thermal and Dielectric Behavior of Polyamide-6/Clay Nanocomposites. *Mater. Chem. Phys.* 232, 99 (2019).
- L. Li, B. Zhou, J. Ye, W. Wu, F. Wen, Y. Xie, and P. Bass, Enhanced Dielectric and Energy-Storage Performance of Nanocomposites Using Interface-Modified Anti-ferroelectric Fillers. *J. Alloys Compd.* 831, 154770 (2020).
- X. Hu, Y. Zhou, J. Liu, and B. Chu, Improved Flexoelectricity in PVDF/Barium Strontium Titanate (BST) Nanocomposites. *J. Appl. Phys.* 123, 154101 (2018).
- N. Meng, X. Zhu, R. Mao, M.J. Reece, and E. Bilotti, Nanoscale Interfacial Electroactivity in PVDF/PVDF-TrFE Blended Films with Enhanced Dielectric and Ferroelectric Properties. *J. Mater. Chem. C* 5, 3296 (2017).
- G. Rajitha, and R.K. Dash, Optically Transparent and High Dielectric Constant Reduced Graphene Oxide (RGO)-PDMS Based Flexible Composite for Wearable and Flexible Sensors. *Sens. Actuators, A: Phys.* 277, 26 (2018).
- M. Guo, J. Jiang, Z. Shen, Y. Lin, C.-W. Nan, and Y. Shen, High-Energy-Density Ferroelectric Polymer Nanocomposites for Capacitive Energy Storage: Enhanced Breakdown Strength and Improved Discharge Efficiency. *Mater. Today* 29, 49 (2019).
- J. Jiang, Z. Shen, J. Qian, Z. Dan, M. Guo, Y. Lin, C.W. Nan, L. Chen, and Y. Shen, Ultrahigh discharge efficiency in Multilayered Polymer Nanocomposites of High Energy Density. *Energy Storage Mat.* 18, 213 (2019).
- M. Kumar, R. Rai, N. Kumar, G. Sharma, A.K. Singh, and S. Kumar, Crystal Structure Correlation of Ferroelectric and Dielectric Properties of Nb Doped PZT95/5. *J. Mater. Sci. Mater. Electron.* 30, 5014 (2019).
- C. Manière, G. Riquet, and S. Marinel, Dielectric Properties of Flash Spark Plasma Sintered BaTiO<sub>3</sub> and CaCu<sub>3</sub>Ti<sub>4</sub>O<sub>12</sub>. *Scr. Mater.* 173, 41 (2019).
- W. Pan, M. Cao, H. Hao, Z. Yao, Z. Yu, and H. Liu, Defect Engineering Toward the Structures and Dielectric Behaviors of (Nb, Zn) Co-Doped SrTiO<sub>3</sub> Ceramics. *J. Eur. Ceram. Soc.* 40, 49 (2020).
- A.K. Abdul Gafoor, M.M. Musthafa, and P.P. Pradyumnan, AC Conductivity and Diffuse Reflectance Studies of Ag-TiO<sub>2</sub> Nanoparticles. *J. Electron. Mater.* 41, 2387 (2012).
- W. Xia, and Z. Zhang, PVDF-Based Dielectric Polymers and Their Applications in Electronic Materials. *IET Nanodielectr.* 1, 17 (2018).
- A. Ahmed, I.A. Goldthorpe, and A.K. Khandani, Electrically Tunable Materials for Microwave Applications. *Appl. Phys. Rev.* 2, 11302 (2015).
- Y. Song, Y. Shen, P. Hu, Y. Lin, M. Li, and C.W. Nan, Significant Enhancement in Energy Density of Polymer Composites Induced by Dopamine-Modified Ba<sub>0.6</sub>Sr<sub>0.4</sub>TiO<sub>3</sub> Nanofibers. *Appl. Phys. Lett.* 101, 152904 (2012).
- Z.B. Pan, L.M. Yao, J.W. Zhai, S.H. Liu, K. Yang, H.T. Wang, and J.H. Liu, Fast Discharge and High Energy Density of Nanocomposite Capacitors Using Ba<sub>0.6</sub>Sr<sub>0.4</sub>TiO<sub>3</sub> Nanofibers. *Ceram. Int.* 42, 14667 (2016).
- Y. Xie, W. Jiang, T. Fu, J. Liu, Z. Zhang, and S. Wang, Achieving High Energy Density and Low Loss in PVDF/BST Nanodielectrics with Enhanced Structural Homogeneity. *ACS Appl. Mater. Interfaces* 10, 29038 (2018).
- M. Feng, Q. Chi, Y. Feng, Y. Zhang, T. Zhang, C. Zhang, Q. Chen, and Q. Lei, High Energy Storage Density and Efficiency in Aligned Nanofiber Filled Nanocomposites with Multilayer Structure. *Compos. B Eng.* 198, 108206 (2020).
- S. Liu, and J. Zhai, A small Loading of Surface-Modified Ba<sub>0.6</sub>Sr<sub>0.4</sub>TiO<sub>3</sub> Nanofiber-Filled Nanocomposites with Enhanced Dielectric Constant and Energy Density. *RSC Adv.* 4, 40973 (2014).
- I.O. Pariy, A.A. Ivanova, V.V. Shvartsman, D.C. Lupascu, G.B. Sukhorukov, M.A. Surmeneva, and R.A. Surmenev, Poling and Annealing of Piezoelectric Poly(Vinylidene Fluoride) Micropillar Arrays. *Mater. Chem. Phys.* 239, 122035 (2020).
- P. Sapkota, S. Ueno, I. Fujii, G.P. Khanal, S. Kim, and S. Wada, Influence of Grain Size Effect and Ba/Ti Ratios on Dielectric, Ferroelectric, and Piezoelectric Properties of BaTiO<sub>3</sub> Ceramics. *Jap. J. Appl. Phys.* 58, SSLC05 (2019).
- M. Feng, C. Zhang, G. Zhou, T. Zhang, Y. Feng, Q. Chi, and Q. Lei, Enhanced Energy Storage Characteristics in PVDF-Based Nanodielectrics with Core-Shell Structured and Optimized Shape Fillers. *IEEE Access* 8, 81542 (2020).
- Prateek, S. Siddiqui, R. Bhunia, N. Singh, A. Garg, and R.K. Gupta, Interface Modulation in Multi-layered BaTiO<sub>3</sub> Nanofibers/PVDF Using the PVP Linker Layer as an Adhesive for High Energy Density Capacitor Applications. *Mater. Adv.* 1(4), 680 (2020).
- X. Xiong, D. Shen, Q. Zhang, H. Yang, J. Wen, and Z. Zhou, Achieving High Discharged Energy Density in pvdf-Based Nanocomposites Loaded with Fine Ba<sub>0.6</sub>Sr<sub>0.4</sub>TiO<sub>3</sub> Nanofibers. *Compos. Commun.* 25, 100682 (2021).
- Z. Wang, T. Wang, C. Wang, Y. Xiao, P. Jing, Y. Cui, and Y. Pu, Poly(Vinylidene Fluoride) Flexible Nanocomposite Films

- with Dopamine-Coated Giant Dielectric Ceramic Nanopowders, Ba(Fe<sub>0.5</sub>Ta<sub>0.5</sub>)O<sub>3</sub>, for High Energy-Storage Density at Low Electric Field. *ACS Appl. Mater. Interfaces* 9, 29130 (2017).
29. Y. Wang, Y. Hou, and Y. Deng, Effects of Interfaces Between Adjacent Layers on Breakdown Strength and Energy Density in Sandwich-Structured Polymer Composites. *Compos. Sci. Technol.* 145, 71 (2017).
  30. R. Bhunia, D. Ghosh, B. Ghosh, S. Hussain, R. Bhar, and A.K. Pal, Some Aspects of Microstructural and Dielectric Properties of Nanocrystalline CdS/Poly(Vinylidene Fluoride) Composite Thin Films. *Polym. Int.* 64, 924 (2015).
  31. R. Senthil Kumar, T. Sarathi, K.K. Venkataraman, and A. Bhatlacharyya, Enhanced Piezoelectric Properties of Polyvinylidene Fluoride Nanofibers Using Carbon Nanofiber and Electrical Poling. *Mater. Lett.* 225, 126515 (2019).
  32. S. Liu, S. Xue, W. Zhang, and J. Zhai, Enhanced Dielectric and Energy Storage Density Induced by Surface-Modified BaTiO<sub>3</sub> Nanofibers In Poly(Vinylidene Fluoride) Nanocomposites. *Ceram. Int.* 40, 15633 (2014).
  33. V. Vinothini, P. Singh, and M. Balasubramanian, Optimization of Barium Titanate Nanopowder Slip for Tape Casting. *J. Mater. Sci.* 41, 7082 (2006).
  34. Z.P. Zheng, S.P. Gong, S.F. Cheng, D.X. Zhou, Y.X. Hu, and H. Liu, Fabrication of BaTiO<sub>3</sub>-Based Semiconducting Ceramic Thick Films by Aqueous Tape Casting. *Key Eng. Mater.* 368–372, 469 (2008).
  35. L. Wang, F. Gao, J. Xu, K. Zhang, J. Kong, M. Reece, and H. Yan, Enhanced Dielectric Tunability and Energy Storage Properties of Plate-Like Ba<sub>0.6</sub>Sr<sub>0.4</sub>TiO<sub>3</sub>/Poly(Vinylidene Fluoride) Composites Through Texture Arrangement. *Compos. Sci. Technol.* 158, 112 (2018).
  36. D.J. Griffiths, *Introduction to electrodynamics* (New Jersey: Prentice Hall, 1962).
  37. C. Baek, J.E. Wang, D.S. Kim, and D.K. Kim, Hydrothermal Synthesis and Dielectric Properties of Ba<sub>1-x</sub>Sr<sub>x</sub>TiO<sub>3</sub> Nanoparticles with Enhanced Uniformity. *J. Nanosci. Nanotechnol.* 16, 11652 (2016).
  38. P. Gupta, A. Kumar, M. Tomar, V. Gupta, and D.P. Singh, Enhanced Dielectric Properties and Suppressed Leakage Current Density of PVDF Composites Flexible Film Through Small Loading of Submicron Ba<sub>0.7</sub>Sr<sub>0.3</sub>TiO<sub>3</sub>Crystallites. *J. Mater. Sci. Mater. Electron.* 28, 11806 (2017).
  39. B.A. Newman, C.H. Yoon, K.D. Pae, and J.I. Scheinbeim, Piezoelectric Activity and Field-Induced Crystal Structure Transitions in Poled Poly(Vinylidene Fluoride) Films. *J. Appl. Phys.* 50, 6095 (1979).
  40. S. Chen, K. Yao, F.E.H. Tay, and C.L. Liow, Ferroelectric Poly(Vinylidene Fluoride) Thin Films on si Substrate With the B Phase Promoted by Hydrated Magnesium Nitrate. *J. Appl. Phys.* 102, 104108 (2007).
  41. X. Cai, T. Lei, D. Sun, and L. Lin, A Critical Analysis of the  $\alpha$ ,  $\beta$  and  $\gamma$  Phases in Poly(Vinylidene Fluoride) Using FTIR. *RSC Adv.* 7, 15382 (2017).
  42. S. Kaur, and D.P. Singh, On the Structural, Dielectric and Energy Storage Behaviour of PVDF- CaCu<sub>3</sub>Ti<sub>4</sub>O<sub>12</sub> Nanocomposite Films. *Mater. Chem. Phys.* 239, 122301 (2020).
  43. Y. Ren, Y. Wang, W. Zhang, X. Yan, and B. Huang, Improved Battery Performance Contributed by the Optimized Phase Ratio of  $\beta$  and  $\alpha$  of PVDF. *RSC Adv.* 9, 29760 (2019).
  44. L. Ruan, X. Yao, Y. Chang, L. Zhou, G. Qin, and X. Zhang, Properties and Applications of the  $\beta$  Phase Poly(Vinylidene Fluoride). *Polym. (Basel)* 10, 1 (2018).
  45. R.I. Mahdi, and W.H. Abd Majid, Piezoelectric and Pyroelectric Properties of bnt-Base Ternary Lead-Free Ceramic-Polymer Nanocomposites Under Different Poling Conditions. *RSC Adv.* 6, 81296 (2016).
  46. R.I. Mahdi, W.C. Gan, N.A. Halim, T.S. Velayutham, and W.H.A. Majid, Ferroelectric and Pyroelectric Properties of Novel Lead-Free Polyvinylidene fluoride-Trifluoroethylene-Bi<sub>0.5</sub>Na<sub>0.5</sub>TiO<sub>3</sub> Nanocomposite Thin Films for Sensing Applications. *Ceram. Int.* 41, 13836 (2015).
  47. C.V. Chanmal, and J.P. Jog, Study of Dielectric Behavior in PVDF/Clay Nanocomposites. *E-Polym.* 9, 1 (2009).
  48. R.K. Goyal, and A.B. Kulkarni, Electrical Properties of Novel Three-Phase Polymer Nanocomposites with a High Dielectric Constant. *J. Phys. D Appl. Phys.* 45, 465302 (2012).
  49. S. Kaur, A.L. Sharma, A. Kumar, and D.P. Singh, Enhanced Dielectric Properties of the Poly(Vinylidene Fluoride)-CaCu<sub>3</sub>Ti<sub>4</sub>O<sub>12</sub> Nanocomposite Thick Films by Quenching in Ice Water. *Mater. Chem. Phys.* 254, 123530 (2020).
  50. C.V. Chanmal, and J.P. Jog, Dielectric Relaxations in PVDF/BaTiO<sub>3</sub> Nanocomposites. *Express Polym. Lett.* 2, 294 (2008).
  51. S. Nayak, and D. Khastgir, Polydimethylsiloxane-PbZr<sub>0.52</sub>Ti<sub>0.48</sub>O<sub>3</sub> Nanocomposites with High Permittivity: Effect of Poling and Temperature on Dielectric Properties. *J. Appl. Polym. Sci.* 136, 47307 (2019).
  52. M. Sharma, A. Gaur, and J.K. Quamara, Temperature-Dependent Dielectric response of (1-x)PVDF/(x)BaTiO<sub>3</sub> Nanocomposite films. *Phys. B Condens. Matter* 563, 23 (2019).
  53. S. Liu, and J. Zhai, Improving the Dielectric Constant and Energy Density of Poly(Vinylidene Fluoride) Composites Induced by Surface-Modified SrTiO<sub>3</sub> Nanofibers by Polyvinylpyrrolidone. *J. Mater. Chem. A* 3, 1511 (2015).
  54. H. Zhang, M.A. Marwat, B. Xie, M. Ashtar, K. Liu, Y. Zhu, L. Zhang, P. Fan, C. Samart, and Z.G. Ye, Polymer Matrix Nanocomposites with 1D Ceramic Nanofillers for Energy Storage Capacitor Applications. *ACS Appl. Mater. Interfaces* 12, 1 (2020).

**Publisher's Note** Springer Nature remains neutral with regard to jurisdictional claims in published maps and institutional affiliations.